Vortex Beam Optimization Design of Concentric Uniform Circular Array Antenna with Improved Array Factor

Qiang Feng, Yifeng Lin, Yushan Zheng, and Long Li *

Key Laboratory of High Speed Circuit Design and EMC of Ministry of Education
School of Electronic Engineering
Xidian University, Xi'an, 710071, China
*lilong@mail.xidian.edu.cn

Abstract ─ In this paper, an improved array factor of the concentric uniform circular array (CUCA) antenna is proposed for the orbital angular momentum (OAM) vortex beam optimization design. From the perspective of the radiation pattern's power conservation principle, a correction factor is introduced to the conventional array factor of CUCA. Then, based on the improved array factor, by adjusting the rings' radii parameters of the CUCA, we optimize the vortex beam's sidelobe level through the generic algorithm (GA). Two different CUCA antenna model are calculated as examples to further illustrate the effectiveness of the improved array factor. Subsequently, an electromagnetic simulation model of two rings CUCA antenna is built at C band for generating low sidelobe vortex beam carrying OAM mode. The electromagnetic simulation model of the designed CUCA antenna is also fabricated and measured. The corresponding antenna far-field vortex beam radiation pattern and near-field vortex wave electric field distributions are measured. The simulation results and the measurement results are in good agreement. The proposed designs of antenna and OAM vortex beam regulation are expected to be used for 5G and 6G communications applications.

Index Terms ─ Concentric uniform circular array (CUCA), Generic algorithm (GA), orbital angular momentum (OAM), sidelobe suppression, uniform circular array (UCA), vortex beam.

I. INTRODUCTION

It has been many years since the concept of the orbital angular momentum (OAM) was presented [1]. In 2007, the OAM was introduced in radio domain through the uniform circular array (UCA) antenna [2], and then it was systematically researched [3]. The OAM was considered to be applied in communication and radar field [4-7], although there were still some controversies about it [8-12]. At the same time, many kinds of OAM vortex wave antennas were developed [13]. The array antenna especially UCA antenna [4, 7] and metasurface antenna [14-17] are comparatively more widely used.

Since the UCA antennas were researched systematically, it was widely researched in wireless communication [4, 18, 19] and radar imaging [7, 20]. However, there are still many important problems needed to be solved [4, 11], and one of them is the vortex beam optimization design, such as the sidelobe suppression. It seems that a few publications consider this issue. In the communication domain, it was referred in [4] that the high peak intensity sidelobe of the vortex beam caused the power dissipation, but no better solutions were presented. In the radar domain, the CUCA antenna [7, 20] were used for vortex beam alignment and sidelobe suppression. In [7], the multiple OAM modes vortex beams' mainlobe alignments were realized by changing the different rings' radii of the CUCA. For different types of single OAM mode vortex beam, in [20], the vortex beam sidelobe suppression and beam collimation were achieved simultaneously through controlling the excitation amplitude of the CUCA with the fixed array radiuses.

Nevertheless, we find some drawbacks that were not evidently noticed in the previous related researches when they design and simulate the UCA antenna models. We note that the UCA array factor used in the traditional design process is inaccurate especially in the CUCA design, which is virtually an approximation. In this paper, we introduce a correction factor (CF) to improve this deficiency. The improved CUCA array factor is utilized in our vortex beam optimization design. Then, through the generic algorithm (GA) optimization about the radius settings of the CUCA, the low sidelobe vortex beam can be realized. The rest parts of this paper are organized as follows. In Section II, the CUCA model is reanalyzed and the correction factor (CF) for the CUCA antenna array factor is presented. Then, it is the specific optimization process and the related analysis through the GA. In Section III, an electromagnetic full-wave simulation model of a two rings CUCA antenna is optimized, designed, and built, based on the improved array factor, and the corresponding vortex beam

Submitted On: November 2, 2020
Accepted On: January 18, 2021
https://doi.org/10.47037/2021.ACES.J.360702

radiation pattern analysis are carried out. Finally, we fabricated the designed two rings CUCA antenna. The corresponding far-field and near-field measurement are finished. Section IV is the conclusion.

II. CONCENTRIC UNIFORM CIRCULAR ARRAY (CUCA) ANTENNA MODEL AND THE GA OPTIMIZATION DESIGN

In this part, the CUCA model's array factors are reanalyzed, and the correction factor (CF) is introduced for improving the accuracy of the CUCA's array factor. Then, based on the improved array factor, a corresponding new fitness function for GA is derived for vortex beam sidelobe suppression optimization design. By optimizing the radius parameters of the CUCA, the best radius parameters are obtained. The corresponding design and optimization processes are also presented in detail.

A. CUCA antenna model re-describe

A general CUCA antenna model is shown in Fig. 1, and the array factor of the single UCA can be written as [3, 21],

$$\begin{aligned} AF_i(\mathbf{r}) &= \sum_{n=0}^{N-1} \frac{1}{\left|\mathbf{r}-\mathbf{r}_n\right|} e^{j\mathbf{k}\left|\mathbf{r}-\mathbf{r}_n\right|} e^{j\ell\varphi_n} \\ &\approx \frac{e^{jkr}}{r} \sum_{n=0}^{N-1} e^{-j\left(k\hat{\mathbf{r}}\cdot\mathbf{r}_n-\ell\varphi_n\right)} \\ &\approx N_i j^{-\ell} \frac{e^{jkr}}{r} e^{j\ell\varphi} J_\ell(ka\sin\theta) \end{aligned}, \tag{1}$$

where $\varphi_n = 2\pi n / N$ is the azimuth angle of the n_{th} array element of the UCA, and ℓ is the OAM mode number. The array factor of the CUCA is,

$$AF_c(\mathbf{r}) = \sum_{i=1}^{m} N_i j^{-\ell} \frac{e^{jkr}}{r} e^{j\ell\varphi} J_\ell(ka_i \sin\theta), \tag{2}$$

where i means the i_{th} ring of the CUCA. Noting that there are some approximations in the formula derivation process: the far-field approximation of $\left|\mathbf{r}-\mathbf{r}_n\right| \approx r - \hat{\mathbf{r}}\cdot\mathbf{r}_n$ for phase approximation, and $\left|\mathbf{r}-\mathbf{r}_n\right| \approx r$ for amplitude approximation. Simultaneously, note that there is also another approximation which is very important that could be ignored, i.e., the Bessel function in (1) is actually obtained when N is large enough. However, if N is not large enough, this approximation will no longer be hold. This problem is not obvious in the single ring UCA design, but it will affect the accuracy of the CUCA's vortex beam design.

We introduce a correction factor (CF) to correct this inaccuracy based on the principle of power conservation. The approximate $AF(\mathbf{r})$ in (1) includes the item $J_\ell(ka\sin\theta)$ whose parameter a will lead to the shape stretch or squeeze of this Bessel function, $J_\ell(ka\sin\theta)$, with its peak value remained unchanged, which is unreasonable compared with the actual UCA antenna radiation. As researched in [3], when the radius of the UCA changes, the obtained radiation pattern gain will also change, i.e., as the UCA radius increases, the gain of the vortex beam also increases. Thus, in order to solve the problem of this inconsistency, we add a correction factor (CF) into the $AF(\mathbf{r})$. The CF is defined as,

$$\begin{aligned} CF(i) &= \sqrt{1/P_i} \\ &= \sqrt{1/\{\frac{1}{N_i}\int_0^{90} AF_i^2(\theta)d\theta\}} \end{aligned}, \tag{3}$$

where P_i is the normalized power which excludes the influence of N_i, the array elements number of the single ring UCA. Considering the symmetry and calculation concise, only quarter space of the radiation pattern, i.e., the angle range from 0 degree to 90 degree, are calculated. Thus, the corrected array factor of the i_{th} ring UCA could be,

$$AF'_i(\mathbf{r}) = AF_i(\mathbf{r}) \cdot CF(i). \tag{4}$$

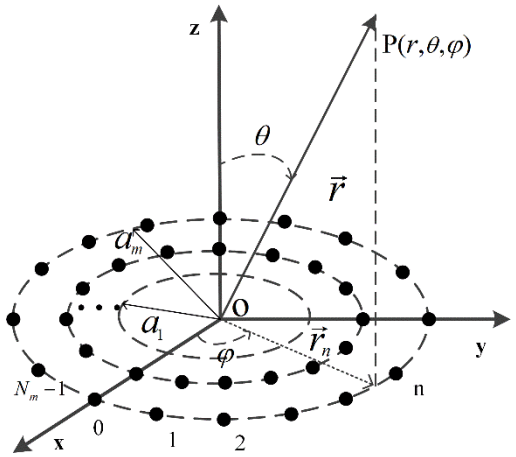

Fig. 1. The CUCA model. It is composed by several rings UCA with different radiuses, a_i. The array element number of each UCA is N_i, $i = 1, 2, \cdots, m$, and m is the ring number of the CUCA.

Then the corresponding array factors of an eight elements UCA antenna model under different radius parameters are calculated. Note that the working frequency is 4.25 Hz with working wavelength of λ = 0.07 m, and the order of the Bessel function is $\ell = 1$ which corresponds to the OAM mode number $\ell = 1$. As shown in Fig. 2, the normalized array factor change curves versus different UCA radii are compared together under the condition whether the CFs are added. As shown in Fig. 2 (a), when the UCA's radius changes, its array factor curve is stretched or squeezed while holding the same peak value. From the perspective of power

conservation, this is unreasonable. Thus, as shown in Fig. 2 (b), the CFs are used. As the UCA's radius changes, the array factor curve's peak value adjusts correspondingly. For example, when the UCA's radius decreases, its radiation pattern will be stretched, and thus the corresponding peak value will turn to be decreased. We remark that the array factor curves calculated with the CFs turn to be more reasonable and more close to the real radiation pattern.

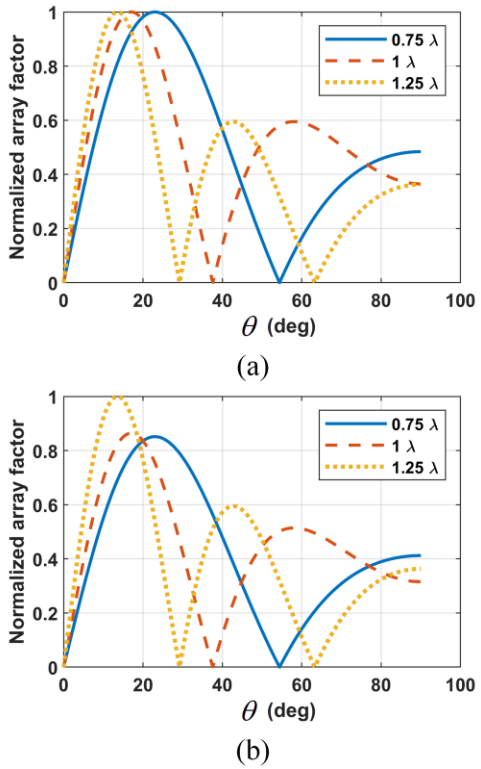

Fig. 2. The normalized array factor change curves under different UCA radiuses, (a) wihtout CF and (b) with CF. Three different UCA radiuses are used here, 0.75λ, 1λ, and 1.25λ.

B. GA optimization design and two calculation examples

In this subsection, based on the improved array factor of the CUCA, the array optimization design for vortex beam's sidelobe suppression through the GA is performed. We describe the corresponding optimization problem and optimization process in detail. Then, two different CUCA antenna models are calculated as the examples to further illustrate the effectiveness of the improved array factor with the correction factor (CF).

The array factor of the CUCA can be rewritten as,

$$AF_c(\mathbf{r}) = \sum_{i=1}^{m}\{N_m j^{-\ell}\frac{e^{jkr}}{r}e^{j\ell\varphi}J_\ell(ka_i\sin\theta)\}\cdot CF(i) = \sum_{i=1}^{m}AF_i(\theta)\cdot CF(i) \quad (5)$$

The fitness function of the GA can be expressed as,

$$f(\mathbf{a}) = P_{side}/P, \quad (6)$$

where $\mathbf{a}=(a_1, a_2, \cdots, a_i)$, P_{side} is the power level of the sidelobe, and P is the peak power level of the CUCA's array factor. Thus, the corresponding optimization problem turns to be as follows,

$$\min\ f(\mathbf{a}) \quad \text{s.t.} \begin{cases} \mathrm{A}\mathbf{a} \le \mathrm{b}, \\ lb_i \le a_i \le ub_i \end{cases}. \quad (7)$$

A is the corresponding coefficient matrix used for restricting the radii of the CUCA's rings. $\mathbf{a}=(a_1, a_2, \cdots, a_i)^{\mathrm{T}}$ is the vector constituted by the radii of the different rings of the CUCA, in which expression $(*)^{\mathrm{T}}$ means the matrix transpose. **b** is the corresponding coefficient vector. **lb** = $(lb_1, lb_2, ..., lb_i)$ and **ub** = $(ub_1, ub_2, ..., ub_i)$ are the low boundary and up boundary constraints of the different rings's radii of the CUCA. All these optimization parameters, including matrix **A**, vector **b**, low boundary **lb**, and up boundary **ub,** are decided by the specific CUCA configurations.

Then, we calculate two examples: one example is a two rings CUCA model, and the other example is a three rings CUCA model. In both these two calculation examples, three different situations are compared, the CUCA's array factor calculated with the CF, the CUCA's array factor calculated without the CF, and the exact array factor calculation using pattern multiplication, i.e., exact calculation. We calculated the two rings CUCA antenna model and three rings CUCA antenna model respectively as follows. Note that the rings' radius parameters are optimized through the GA, and the optimized array factor with the CF is adopted here. The corresponding GA optimize processes are mainly realized by the optimization tool in MATLAB. The main related parameters configurations about the GA are listed in Table 1, and the other related optimization parameters are default. Note that for the Mutation function and Crossover function, the default options 'Constraint dependent' was adopted in the 'optimtool' of MATLAB.

Table 1: The relevant parameters settings of GA in MATLAB

Population Size	Optimization Variable Number	Crossover Fraction	Mutation Function	Crossover Function	Stopping Criteria	
					Generations	Function Tolerance
50	2 or 3	0.8	'Constraint dependent'	'Constraint dependent'	Optimization variable number × 100	$10^{(-6)}$

For three rings CUCA antenna model, it has 8 array elements, 14 array elements and 20 array elements for each ring. The boundary constraints adopted here in the GA optimization are set as,

$$\mathbf{A} = \begin{bmatrix} 1 & -1 & 0 \\ 0 & 1 & -1 \end{bmatrix}, \ \mathbf{b} = \begin{bmatrix} -0.025 \\ -0.025 \end{bmatrix},$$
$$\mathbf{lb} = (0.045, 0.07, 0.095), \quad (8)$$
$$\mathbf{ub} = (0.12, 0.12, 0.14).$$

Note that the length unit used here is meter and the working frequency is 4.25 GHz with working wavelength of 0.07 m. For the two rings CUCA antenna model with 8 elements and 14 elements, its boundary constraints adopted in the GA optimization are set as,

$$\mathbf{A} = \begin{bmatrix} 1 & -1 \end{bmatrix}, \ \mathbf{b} = \begin{bmatrix} -0.025 \end{bmatrix},$$
$$\mathbf{lb} = (0.045, 0.07), \quad (9)$$
$$\mathbf{ub} = (0.12, 0.12).$$

Note that all these parameters are selected based on the given CUCA antenna model's configurations, which considers the factors such as the interval space between the array elements, the interval space between the different UCA rings, and the amount of the array elements of the CUCA.

After performing the GA optimization, we obtain the optimized radius parameters of the CUCA models as follows. For the two rings CUCA model, we select the optimized radiuses parameters as 45 mm and 86 mm. The calculated array factor curves under three different situations are compared together in Fig. 3 (a). For the three rings CUCA model, its optimized radiuses of the three rings are 47.2 mm, 71.2 mm, and 112.3 mm respectively. The calculated array factor curves are compared in Fig. 3 (b) as follows. From these two calculation examples, it is obvious that the array factor curve calculated with adding the CF is closer to the exact calculation results. For the calculated array factor with CF, although there are still some inconsistencies, its main radiation pattern parameters, such as the mainlobe's beam width, and the sidelobe's zero positions, are more consistent with the array factor calculated under the exact calculation.

Noting that the CUCA model used in this paper is an ideal antenna model, and we mainly solve this problem from a pure mathematical perspective. Although only the array factor of the antenna array is considered, however, it usually has an important weight in antenna array design. In practical antenna design and optimization design process, the array antenna design theory must be followed.

For example, in this paper, N is the array element number of each UCA. From a pure mathematical perspective, N is arbitrary, however, in practical antenna design process, the actual antenna size limit, as well as the array antenna elements' interval distance and their mutual coupling constraints, all these factors will restrict the number of N. In practical optimization design, the applicable range of N is usually determined by the actual antenna array model. Moreover, for the GA optimization, the selection of the boundary constraints is also important, different boundary constraints selection could lead to different optimization results.

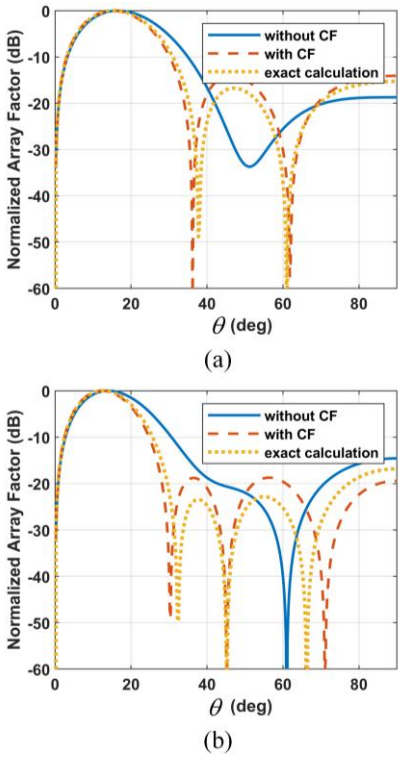

Fig. 3. Comparison about the calculated array factors of two rings CUCA and three rings CUCA under these three different situations, without the correction factor (CF), with the correction factor (CF), and exact calculation. (a) The two rings CUCA antenna model; (b) the three rings CUCA antenna model.

III. ARRAY ANTENNA SIMULATION AND MEASUREMENT

In this part, the electromagnetic (EM) simulation models of the CUCA antenna with the optimized rings' radii is built through EM simulation software ANSYS HFSS to realize low sidelobe vortex beam design with OAM mode number $\ell = 1$ at center frequency 4.25 GHz. Two other antenna array models are also built as references: One model is a single ring UCA antenna, and the other model is a double rings CUCA antenna whose ring radiuses are different from the optimized radius parameters values. Finally, the optimized CUCA antenna is fabricated, and it is measured in both far-field and near-field environment.

A. Array antenna simulation

Considering the electromagnetic simulation model construction and the ease of the prototype fabrication and measurement, we optimized another two rings CUCA antenna model with eight elements for each rings. Adopting the GA optimization process mentioned above, based on the improved array factor of the CUCA, finally, we select a group optimized radius parameters, 54 mm and 98 mm, as our design parameters for the simulated EM simulation model of the two rings CUCA antenna.

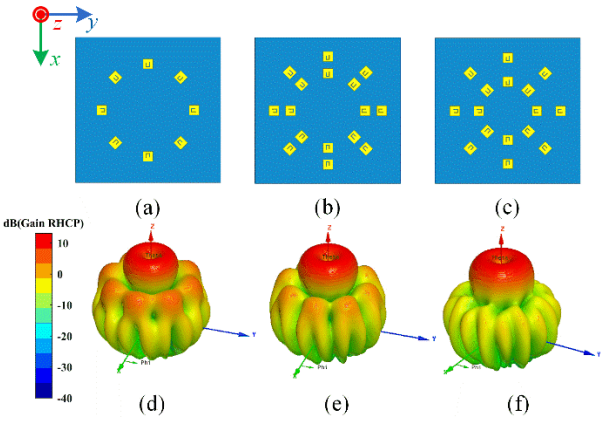

Fig. 4. The size of the array are all same with 260 mm × 260 mm × 2 mm, and the substrate used here is F4B whose $\varepsilon_r = 2.65$. (a) The single ring UCA whose radius is 86 mm; (b) the double rings CUCA, a_1 = 69 mm, and a_2 = 100 mm; (c) the optimized CUCA, a_1 = 54 mm, and a_2 = 99 mm; (d)-(f) the simulated 3D radiation patterns.

Together with the other two reference array antenna model, these three different EM simulation models are shown in Figs. 4 (a)-(c), whose 3D far-field radiation patterns are shown in Figs. 4 (d)-(f). What needs to be mentioned here is that a center feeding right hand circular polarization (RHCP) antenna is used as the array element to simplify the later feeding network design, because an optional excitation phase of the array element can be easily realized by centrally rotating the certain angle of the antenna element [22, 23]. But for brevity, it is not exhibited here in detail. In Fig. 5, the 2D radiation gain pattern of these three different array antenna models are compared together. The optimization array with sidelobe suppression has slightly larger gain than the other two models' gain. The optimized CUCA antenna does work, whose sidelobe level is obviously better than the other two reference models, and it obtains nearly -15 dB vortex sidelobe level.

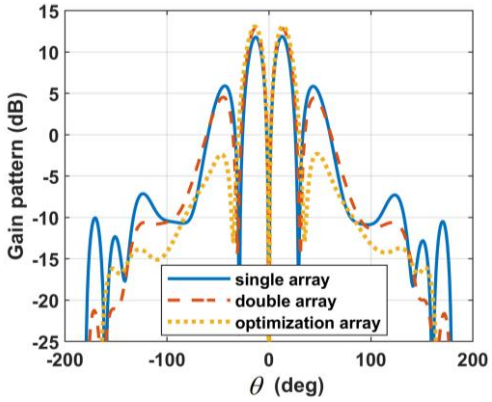

Fig. 5. The 2D radiation gain pattern comparisons between the three different CUCA antenna models. The exact maximum gain values of the single array, double array, and optimization array are 11.8 dB, 12.8 dB, and 13.1 dB respectively.

B. Array antenna measurement

The fabricated prototype corresponding to the CUCA model in Fig. 4 (c) is shown in Fig. 6. A 16 ways power divider module is used for antenna array feeding, which was connected to the antenna array by the same RF cables with same length. Before the actual test in the microwave anechoic chamber, the S11 of the prototype antenna is measured as shown in Fig. 7, which satisfies the general engineering requirements.

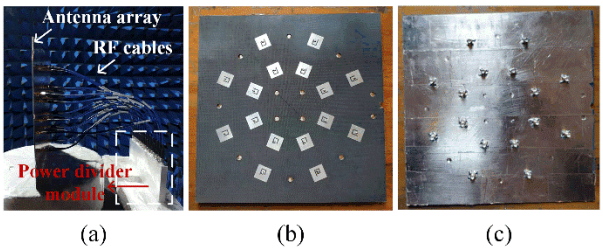

Fig. 6. (a) The whole prototype of the antenna array with the feeding network. The size of the array prototype is 260 mm × 260 mm × 2 mm. (b) Top side view, and (c) bottom side view.

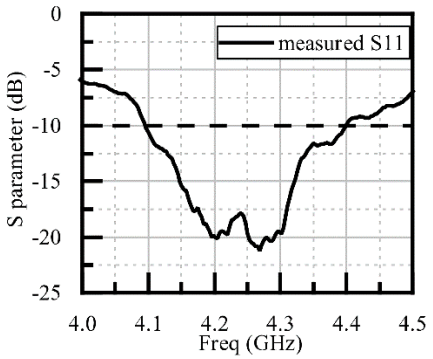

Fig. 7. The measured S_{11} of the prototype antenna.

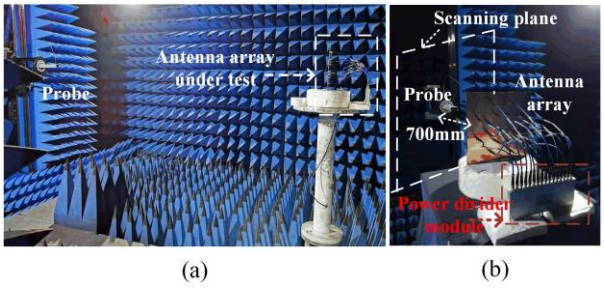

Fig. 8. (a) The far-field measurement environment. (b) The near-field measurement environment, and the distance between the measurement probe and the antenna array is 700 mm, the scanning plan is 800 mm × 800 mm with sample period of 16 mm leading to 51 ×51 sampling grid.

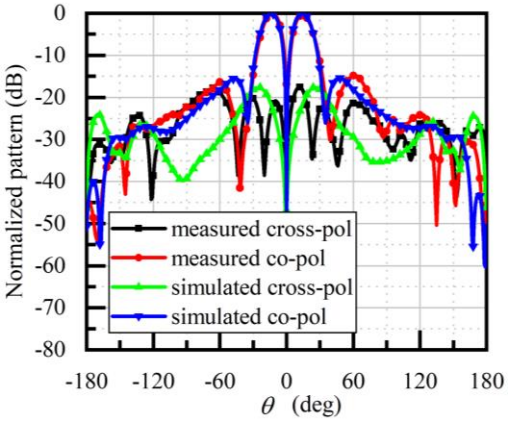

Fig. 9. The 2D radiation pattern comparisons between the simulated results and the measured results.

The far-field and near-field measurement environment are shown in Figs. 8 (a) and (b) respectively. In Fig. 9, the simulated 2D radiation pattern and the measured results are compared together, which are consistent. It can be seen that a nearly -15 dB sidelobe level is realized. Finally, the vortex beam electric field distributions are measured and they are compared with the simulation results as shown in Fig. 10, which are consistent well. From Figs. 10 (a) and (b), it is obvious that the typical 'doughnut' shape electric field distribution and spiral phase distribution are obtained, and the circular polarization OAM vortex wave carrying OAM mode number $\ell = 1$ is realized. In Fig. 11, it performs a further OAM mode purity analysis [24] about the measured vortex electric field, in which the principal OAM mode component of OAM mode number $\ell = 1$ is obviously higher than the other modes about 18 dB.

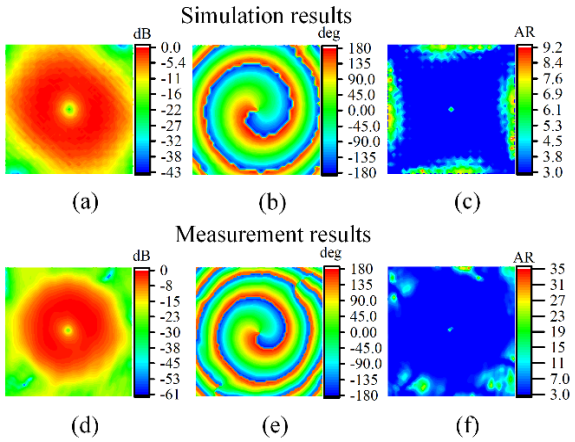

Fig. 10. The simulated and the measured vortex electric field distributions. The simulated observation plane has same size as the measurement, and the distance between the observation plane and the array is same as the measurement situation. (a) Intensity distribution, (b) phase distribution, (c) axial ratio (AR) distribution. The areas with dark blue color means that the value of the AR is less than 3dB, and (d)-(f) is the measurement results.

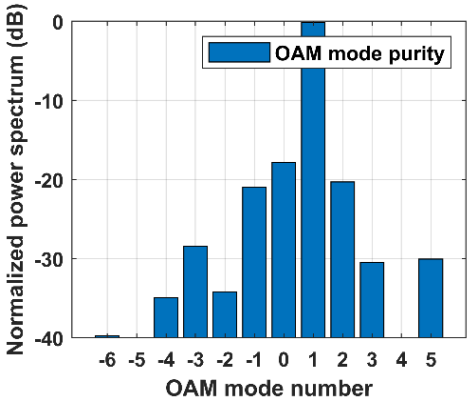

Fig. 11. The calculated OAM mode purity of the measurement vortex electric field, and the normalized OAM mode power means the power of different OAM modes that are normalized by the total received OAM mode power.

IV. CONCLUSION

To summarize, considering the inaccuracies about the approximate array factor calculation of the CUCA antenna, we introduced a correction factor to improve it from the viewpoint of the antenna's radiation pattern power conservation. The corresponding illustrations and the calculation examples were also provided in detail. In order to realize the vortex beam optimization design such as the sidelobe suppression, the GA was adopted to optimize the CUCA's radius parameters. Relevant EM simulation model were built, fabricated and measured. The corresponding far-field and near-field antenna measurements were carried out in microwave anechoic chamber, which showed that the optimized low sidelobe vortex beam was realized. Not limited to the sidelobe suppression, this design method about the vortex beam optimization design, could be applied in the wireless communication field and radar field in the future.

ACKNOWLEDGMENT

This work is supported by National Key R&D Program of China.

REFERENCES

[1] A. M. Yao and M. J. Padgett, "Orbital angular momentum: Origins, behavior and applications," *Advances in Optics and Photonics*, vol. 3, no. 2, pp. 161-204, 2011.

[2] B. Thide, H. Then, J. Sjoholm, K. Palmer, J. Bergman, T. D. Carozzi, Y. N. Istomin, N. H. Ibragimov, and R. Khamitova, "Utilization of photon orbital angular momentum in the low-frequency radio domain," *Phys. Rev. Lett.*, vol. 99, no. 8, pp. 087701, Aug. 24, 2007.

[3] S. M. Mohammadi, L. K. S. Daldorff, J. E. S. Bergman, R. L. Karlsson, B. Thide, K. Forozesh, T. D. Carozzi, and B. Isham, "Orbital angular momentum in radio—A system study," *IEEE Transactions on Antennas and Propagation*, vol. 58, no. 2, pp. 565-572, 2010.

[4] D. Lee, H. Sasaki, H. Fukumoto, K. Hiraga, and T. Nakagawa, "Orbital angular momentum (OAM) multiplexing: an enabler of a new era of wireless communications," *IEICE Transactions on Communications*, vol. E100.B, no. 7, pp. 1044-1063, 2017.

[5] A. Trichili, K.-H. Park, M. Zghal, B. S. Ooi, and M.-S. Alouini, "Communicating using spatial mode multiplexing: Potentials, challenges, and perspectives," IEEE Communications Surveys & Tutorials, vol. 21, no. 4, pp. 3175-3203, 2019.

[6] G. Guo, W. Hu, and X. Du, "Electromagnetic vortex based radar target imaging," (in Chinese), *Journal of National University of Defense Technology*, vol. 6, pp. 71-76, 2013.

[7] T. Yuan, H. Wang, Y. Qin, and Y. Cheng, "Electromagnetic vortex imaging using uniform concentric circular arrays," *IEEE Antennas and Wireless Propagation Letters*, vol. 15, pp. 1024-1027, 2016.

[8] O. Edfors and A. J. Johansson, "Is orbital angular momentum (OAM) based radio communication an unexploited area?," *IEEE Transactions on Antennas and Propagation*, vol. 60, no. 2, pp. 1126-1131, 2012.

[9] M. Tamagnone, C. Craeye, and J. Perruisseau-Carrier, "Comment on 'Encoding many channels on the same frequency through radio vorticity: first experimental test'," *New Journal of Physics*, vol. 14, no. 11, 2012.

[10] F. Tamburini, B. Thidé, E. Mari, A. Sponselli, A. Bianchini, and F. Romanato, "Reply to comment on 'Encoding many channels on the same frequency through radio vorticity: First experimental test'," *New Journal of Physics*, vol. 14, no. 11, 2012.

[11] M. Oldoni, F. Spinello, E. Mari, G. Parisi, C. G. Someda, F. Tamburini, F. Romanato, R. A. Ravanelli, P. Coassini, and B. Thide, "Space-division demultiplexing in orbital-angular-momentum-based MIMO radio systems," *IEEE Transactions on Antennas and Propagation*, vol. 63, no. 10, pp. 4582-4587, 2015.

[12] M. Andersson, E. Berglind, and G. Björk, "Orbital angular momentum modes do not increase the channel capacity in communication links," *New Journal of Physics*, vol. 17, no. 4, 2015.

[13] Z. Guo, Y. Wang, Q. Zheng, C. Yin, Y, Yang, and Y. Gong, "Advances of research on antenna technology of vortex electromagnetic waves," (in Chinese), *Journal of Radars*, vol. 8, no. 5, pp. 631-655, Sep. 2019.

[14] J. Q. Han, L. Li, H. Yi, and Y. Shi, "1-bit digital orbital angular momentum vortex beam generator based on a coding reflective metasurface," *Optical Materials Express*, vol. 8, no. 11, pp. 3470-3478, 2018.

[15] J. Q. Han, L. Li, H. Yi, and W. M. Xue, "Versatile orbital angular momentum vortex beam generator based on reconfigurable reflective metasurface," *Japanese Journal of Applied Physics*, vol. 57, no. 12, 2018.

[16] F. Bi, Z. Ba, and X. Wang, "Metasurface-based broadband orbital angular momentum generator in millimeter wave region," *Opt Express*, vol. 26, no. 20, pp. 25693-25705, 2018.

[17] R. Xie, G. Zhai, X. Wang, D. Zhang, L. Si, H. Zhang, and J. Ding, "High-efficiency ultrathin dual-wavelength pancharatnam–berry metasurfaces with complete independent phase control," *Advanced Optical Materials*, vol. 7, no. 20, p. 1900594, 2019.

[18] R. Chen, H. Xu, M. Moretti, and J. Li, "Beam

steering for the misalignment in UCA-based OAM communication systems," *IEEE Wireless Communications Letters*, vol. 7, no. 4, pp. 582-585, 2018.

[19] R. Chen, H. Zhou, M. Moretti, X. Wang, and J. Li, "Orbital angular momentum saves: Generation, detection, and emerging applications," *IEEE Communications Surveys & Tutorials*, vol. 22, no. 2, pp. 840-868, 2020.

[20] Y. Qin, K. Liu, Y. Cheng, X. Li, H. Wang, and Y. Gao, "Sidelobe suppression and beam collimation in the generation of vortex electromagnetic waves for radar imaging," *IEEE Antennas and Wireless Propagation Letters*, vol. 16, pp. 1289-1292, 2017.

[21] T. Yuan, Y. Cheng, H. Wang, and Y. Qin, "Mode characteristics of vortical radio wave generated by circular phased array: Theoretical and experimental results," *IEEE Transactions on Antennas and Propagation*, vol. 65, no. 2, pp. 688-695, 2017.

[22] L. Li and X. Zhou, "Mechanically reconfigurable single-arm spiral antenna array for generation of broadband circularly polarized orbital angular momentum vortex waves," *Sci. Rep.*, vol. 8, no. 1, p. 5128, 2018.

[23] J. Liang, Z. L. Jing, Q. Feng, Y. S. Zheng, and L. Li, "Synthesis and measurement of a circular-polarized deflection OAM vortex beam with sidelobe suppression array," *IEEE Access*, vol. 8, pp. 89143-89151, 2020.

[24] Q. Feng, J. Liang, and L. Li, "Variable scale aperture sampling reception method for multiple orbital angular momentum modes vortex wave," *IEEE Access*, vol. 7, pp. 158847-158857, 2019.